© 2014. Published by The Company of Biologists Ltd | The Journal of Experimental Biology (2014) 217, 1955-1962 doi:10.1242/jeb.098384

RESEARCH ARTICLE

Mexican blind cavefish use mouth suction to detect obstacles

Roi Holzman[1,2,*], Shimrit Perkol-Finkel[3] and Gregory Zilman[3]

ABSTRACT

Fish commonly use their lateral line system to detect moving bodies such as prey and predators. A remarkable case is the Mexican blind cavefish *Astyanax fasciatus*, which evolved the ability to detect non-moving obstacles. The swimming body of *A. fasciatus* generates fluid disturbances, the alteration of which by an obstacle can be sensed by the fish's lateral line system. It is generally accepted that these alterations can provide information on the distance to the obstacle. We observed that *A. fasciatus* swimming in an unfamiliar environment open and close their mouths at high frequency (0.7–4.5 Hz) in order to generate suction flows. We hypothesized that repeated mouth suction generates a hydrodynamic velocity field, which is altered by an obstacle, inducing pressure gradients in the neuromasts of the lateral line and corresponding strong lateral line stimuli. We observed that the frequency and rate of mouth-opening events varied with the fish's distance to obstacles, a hallmark of pulse-based navigation mechanisms such as echolocation. We formulated a mathematical model of this hitherto unrecognized mechanism of obstacle detection and parameterized it experimentally. This model suggests that suction flows induce lateral line stimuli that are weakly dependent on the fish's speed, and may be an order of magnitude stronger than the correspondent stimuli induced by the fish's gliding body. We illustrate that *A. fasciatus* can navigate non-visually using a combination of two deeply ancestral and highly conserved mechanisms of ray-finned fishes: the mechanism of sensing water motion by the lateral line system and the mechanism of generating water motion by mouth suction.

KEY WORDS: Canal neuromasts, Distant touch, Navigation

INTRODUCTION

The Mexican blind cavefish, *Astyanax fasciatus* (Cuvier 1819) lost its eyes over the course of evolution following multiple independent colonization events of underground caves. It is nonetheless able to successfully avoid obstacles and navigate by utilizing hydrodynamic cues created by its own motion (Dijkgraaf, 1933; Dijkgraaf, 1947; Dijkgraaf, 1963). A moving fish creates hydrodynamic disturbances, namely fluid velocity and pressure fields, which vary with the distance to an obstacle. It has been hypothesized that to form the hydrodynamic image of an obstacle, the fish performs mapping of the hydrodynamic fields into the distance to the obstacle (Campenhausen et al., 1981; Dijkgraaf, 1933; Dijkgraaf, 1947; Dijkgraaf, 1963).

Like other ray-finned fishes, *A. fasciatus* can sense hydrodynamic disturbances using its lateral line, a specialized system of mechanoreceptors located along the fish's head and body (Bleckmann, 2007; Montgomery et al., 1995). The lateral line consists of mechanoreceptors protruding from the skin (superficial neuromasts) and mechanoreceptors located in canals beneath the skin (canal neuromasts). Superficial neuromasts measure the velocity of the flow very close to the skin, while canal neuromasts measure the water pressure difference between adjacent pores in the canal (Denton and Gray, 1983; Denton and Gray, 1988; Denton and Gray, 1989; Denton and Gray, 1982; Kroese and Schellart, 1992). Although surface and canal neuromasts have overlapping functions, blind cave fish can still locate objects even with disabled surface neuromasts (Montgomery et al., 2001), whereas the ability of these fish to navigate with disabled canal neuromasts is impaired or even lost (Abdel-Latif et al., 1990). The pressure difference δp between two adjacent pores of the lateral line is generally considered as a hydrodynamic signal, which also varies with the distance to a wall h (Windsor et al., 2010). For a fish moving steadily in an unbounded fluid, δp is constant. In the presence of an obstacle, δp varies in time. As long as the fish is able to sense and analyze these variations, it is able to detect an obstacle.

Given that the pressure created by the motion of a body in fluid is proportional to the body's square speed, faster Mexican blind cavefish should detect an obstacle sooner and start the avoidance maneuver earlier, at a greater distance from the obstacle. However, turning distances of *A. fasciatus* from a wall were uncorrelated with its swimming speed (Teyke, 1985; Windsor et al., 2008). The apparent disparity was explained as being the result of a fish's analysis of the relative, rather than the absolute, magnitude of the pressure difference (Windsor et al., 2008). In the scientific literature, the gliding body of a fish is considered as the only source of variation in δp with distance to the obstacle. These pressure variations are denoted here as δp_B. To the best of our knowledge, alternative hydrodynamic mechanisms of obstacle detection, in which the stimuli that trigger an obstacle-avoiding maneuver are weakly dependent on a fish's speed, are currently unknown.

Virtually all fish use mouth suction, an evolutionarily conserved and deeply ancestral method for prey capture and transport among teleosts (Lauder, 1980; Lauder, 1982; Lauder, 1985). To generate suction, fish rapidly open the mouth and expand the buccal cavity, generating fast flows and steep pressure gradients that extend in front of the mouth (Day et al., 2005; Day et al., 2007; Higham et al., 2006; Holzman et al., 2008; Weihs, 1980). The mouth is then rapidly closed, and the time from the onset of mouth opening until closing (hereafter 'mouth-opening event') takes 10–100 ms (Gibb and Ferry-Graham, 2005). The same biomechanical mechanism is used to generate respiratory flows, which are characterized by much slower flows and weak accelerations (Brainerd and Ferry-Graham, 2006). In the context of suction feeding, it has been previously shown that the fluid velocity fields change with the distance to a wall (Nauwelaerts et al., 2007; Van Wassenbergh and Aerts, 2009). In other words, mouth suction could provide an independent source of variation in δp with distance to the obstacle. Such pressure differences are denoted here as δp_S. We hypothesize that mouth

[1]Department of Zoology, Faculty of Life Sciences, Tel Aviv University, Tel Aviv 69978, Israel. [2]The Inter-University Institute for Marine Sciences, POB 469, Eilat 88103, Israel. [3]School of Mechanical Engineering, Faculty of Engineering, Tel Aviv University, Tel Aviv 69978, Israel.

*Author for correspondence (holzman@post.tau.ac.il)

Received 14 October 2013; Accepted 3 March 2014

The Journal of Experimental Biology (2014) doi:10.1242/jeb.098384

List of symbols and abbreviations

∇	differential operator of gradient
a, b, c	semi-axes of an equivalent ellipsoid
BL	body lengths
G	instantaneous mouth gape
G_{max}	peak mouth gape
h	instantaneous distance from the plane of the mouth aperture to a plane wall
h_0	initial distance from the plane of the mouth aperture to a plane wall
h_E	distance from the plane of the mouth to the wall when the suction-induced stimulus attains its maximum
h_{min}	minimal distance at which fish starts the wall-avoiding maneuver
I	symbolic notation of mirror image of fish
L	fish length
p	fluid pressure
PIV	particle image velocimetry
$\dot{q}$	flow rate through mouth aperture
r	equivalent radius of the mouth aperture
R	symbolic notation of fish
SNR	signal-to-noise ratio
t	time
T	time to mouth peak gape
t_0	initial time of water suction
U	fish speed
$\mathbf{V}$	fluid velocity vector
v_{max}	maximum velocity of peak intake flow through the mouth aperture
xyz	coordinates of the fish-body-fixed orthogonal coordinate system O_1xyz
δp	pressure difference between two adjacent canal pores
δp_B	pressure difference between two adjacent canal pores induced by body motion
δp_S	pressure difference between two adjacent canal pores induced by mouth suction
δs	distance between two adjacent pores
ν	water kinematic viscosity
$\xi\eta\zeta$	coordinates of the mirror-image-fixed orthogonal coordinate system $O\xi\eta\zeta$
ρ	water density
φ_B	the fluid velocity potential induced by the motion of the fish's body
φ_S	the fluid velocity potential induced by mouth suction
$\bar{\omega}$	the euclidean distance from the central axis of the disc of the mouth to the fluid point

suction can potentially be utilized to detect obstacles using mapping of δp_S to the distance to an obstacle.

Our objective was to test whether mouth suction can be used as an additional hydrodynamic mechanism of obstacle detection in Mexican blind cavefish. Specifically, we asked whether mouth suction in *A. fasciatus* is performed in the absence of food, and whether the rate of mouth-opening events is modulated as a function of the environment. Lastly, we quantified the magnitude of the pressure gradient δp_S resulting from mouth suction and compared it with that resulting from the translating body δp_B.

RESULTS

Experimental results

Swimming freely in a familiar aquarium with no food and under well-ventilated conditions (10.6–10.1 mg O_2 l^{-1}), *A. fasciatus* had a mean (±s.d.) speed U of 0.75±0.23 body lengths (BL) s^{-1} (equivalent to 52.5±16.2 mm s^{-1}). In the familiar environment, fish opened and closed their mouths at a mean frequency of 0.2±0.23 Hz (N=30, maximum 1.08 Hz). After the obstacles in the tank were shifted to arbitrary locations, mouth-opening frequency increased significantly

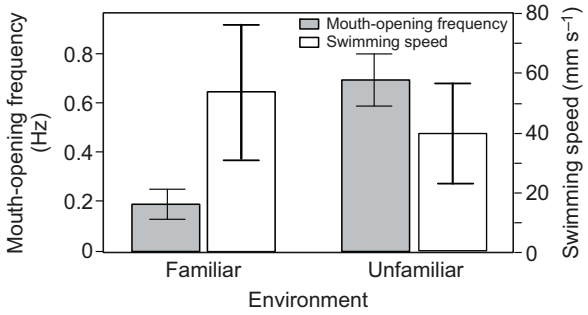

Fig. 1. Mouth-opening frequency and swimming speed in an unfamiliar versus familiar environment. Mouth-opening frequency in *Astyanax fasciatus* increased significantly in an unfamiliar compared with a familiar environment (gray bars; *t*-test, P<0.001, N=61), while swimming speed was lower in an unfamiliar compared with a familiar environment (white bars; *t*-test, P<0.006, N=54). Fish were filmed in a familiar aquarium, then obstacle positions were shifted arbitrarily to create an unfamiliar environment.

(Fig. 1; *t*-test, d.f.=60, P<0.001) by ~3.5-fold to a mean of 0.7±0.65 Hz (N=31, maximum 1.82 Hz) while swimming speed decreased significantly to 0.55±0.26 BL s^{-1} (equivalent to 38.5±18.6 mm s^{-1}; *t*-test, d.f.=53, P<0.006). Within treatments, variance in mouth-opening frequency was not significantly different between individuals (Bartlett's test for homogeneity of variance, d.f.=2, P>0.8).

In a separate set of experiments we focused on mouth-opening events that occurred when the fish swam towards the corner wall of the aquarium (Fig. 2). Fourier analysis revealed that the frequency of these events at a distance h of 110–0 mm from the corner wall was 4.5 Hz (Fig. 2, Fig. 3A). The distribution of mouth-opening events with respect to the distance from the corner, perpendicular to the direction of motion, was significantly different from uniform (χ^2=61.31, d.f.=10, P<0.001). Mouth-opening events were infrequent at a distance greater than 70 mm from the wall; their frequency doubled when the fish were at a distance of 70>h>10 mm, and was more than 6-fold higher at the closest distance (10 mm) to the corner (Fig. 3B).

High-speed videos taken during particle image velocimetry (PIV) experiments (1000 frames s^{-1}) indicate that the maximal mouth gape size G_{max} averaged 2.2±0.7 mm and time to peak mouth opening T averaged 78±51 ms (N=14; Fig. 4A, Table 1). The mouth returned to a closed state after an additional 85±61 ms. High-speed PIV (supplementary material Movie 2) indicated that peak flow speed at the center of the mouth v_{max} averaged 66±22 mm s^{-1} (N=14; range 22–110 mm s^{-1}; Fig. 4B, Table 1).

Results of the mathematical modeling

Fig. 5A illustrates that the pressure difference δp_B induced by the gliding body increases monotonically with decreasing distance to the wall h, as expected (e.g. Milne-Thomson, 1968) [similar results for a fish-like body of revolution are shown in Windsor et al. (Windsor et al., 2010)]. Fig. 5A also illustrates that in each suction event the pressure difference induced by mouth opening oscillates with the distance to the wall h and reaches positive and negative extrema $\delta p_S(h_E)$ at certain distances from the wall, h=h_E. The absolute values of the extrema also grow with decreasing distance to the wall. The larger of the extrema may be two orders of magnitude higher than the pressure difference induced by the gliding body in the range of swimming speeds we observed (10–100 mm s^{-1}). In other words, the wall-detection stimuli induced by mouth suction may be much higher than those induced by the gliding body (Fig. 5A,B).

The Journal of Experimental Biology (2014) doi:10.1242/jeb.098384

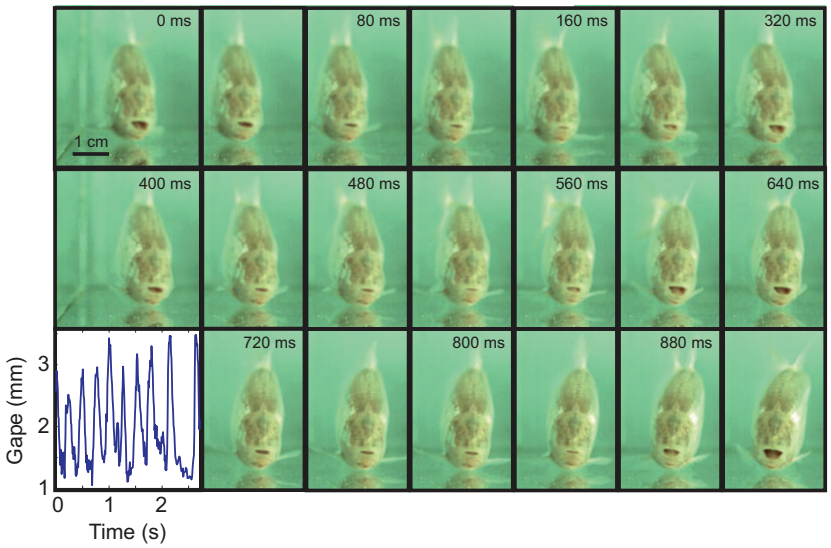

Fig. 2. Repeated mouth opening in *A. fasciatus* approaching a wall in an unfamiliar environment. Data were digitized from supplementary material Movie 1. The original movie was filmed at 125 Hz. The image sequence depicts every 10th frame from the first frame of the movie. Bottom left panel is a frame-by-frame digitization of gape size for the entire movie. The fish swims at a speed of 57 mm s^{-1} and starts turning at t=2.75 s.

It follows from the Euler equations of water motion used to simulate the fluid motion (see Eqn 2 in Materials and methods) that the pressure difference induced by the gliding body $|\delta p_B|$ is proportional to U^2 (e.g. Milne-Thomson, 1968) [similar results for a fish-like body of revolution are shown in Windsor et al. (Windsor et al., 2010)]. The results of mathematical modeling also show that, for the flow parameters adopted here, the pressure difference induced by fast mouth opening $|\delta p_S|$ is weakly dependent on a fish's speed. Therefore, the ratio of maximum $|\delta p_S(h_E)|$ to $|\delta p_B(h_E)|$ is proportional to U^{-2}. From Fig. 5B it is clear that for relatively low swimming speed (U≈20 mm s^{-1}) the detection signal induced by mouth suction is much stronger than the corresponding body-induced signal.

Additionally, in 14 mouth-opening events for which suction flow speed, swimming speed and distance were available from PIV measurements (Table 1), the detection signals due to mouth suction were ~50-fold stronger than those due to the gliding body (Fig. 5C; range 6–233, t-test, t=3.18, d.f.=13, P<0.0071).

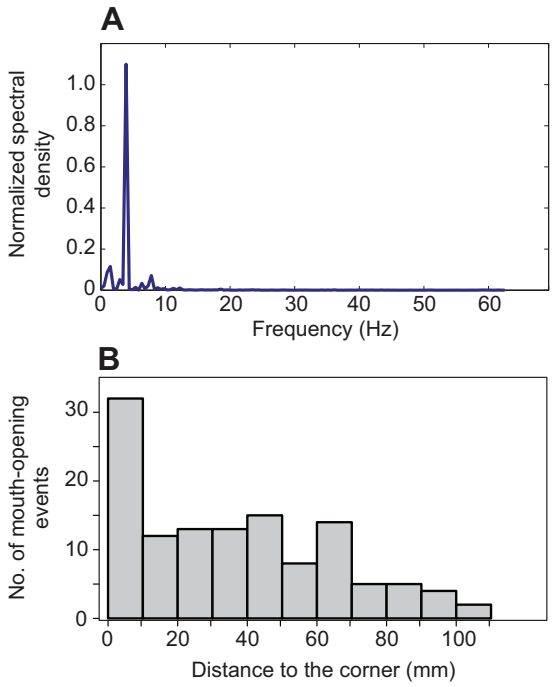

Fig. 3. Modulation of mouth-opening frequencies in an unfamiliar environment (A) Fourier analysis of mouth-opening events, recorded when the fish swam towards the corner wall of the aquarium. Data are from supplementary material Movie 1, which captured mouth-opening events at a distance of 110–0 mm from the corner wall. (B) Frequency distribution of 123 mouth-opening events. Frequency increased as a function of decreasing distance to the wall of the corner. Fish were filmed swimming towards the corner in an unfamiliar environment at 125 frames s^{-1}. The field of view started at a distance of ~110 mm from the corner. Distances from the wall are binned by 10 mm increments.

DISCUSSION

In this paper we propose a new mechanism for non-visual navigation in *A. fasciatus*. We suggest that Mexican blind cavefish repeatedly generate mouth suction flows (Figs 1–3) to produce pressure signals that can be used to detect non-moving obstacles (Fig. 5). Using experimental observations and mathematical modeling we illustrate that for *A. fasciatus* approaching a wall, the pressure difference δp_S between two adjacent canal pores due to mouth suction may be an order of magnitude stronger than the

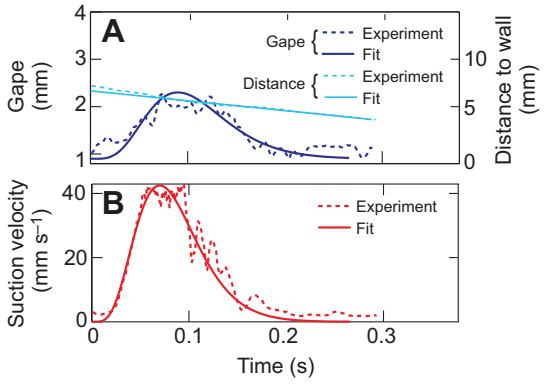

Fig. 4. Kinematics and hydrodynamics of mouth suction in *A. fasciatus* (A) A mouth-opening event from particle image velocimetry (PIV) experiments. The fish glides forward at a speed of U=0.012 m s^{-1} when the mouth opens. (B) Water suction velocity in the center of the mouth aperture measured using PIV. The observed gape size G_{max} and suction velocity in the center of the mouth aperture v_{max} were fitted with a continuous function $A_{max}f(t)$, where A_{max} denotes G_{max} or v_{max}, and $f(t)$ is a continuous function depending on time t (Muller et al., 1982); see Appendix.

The Journal of Experimental Biology (2014) doi:10.1242/jeb.098384

Table 1. Mouth opening and flow suction parameters obtained for 14 PIV measurements

G_{max} (mm)	T (ms)	v_{max} (mm s^{-1})	h_0 (mm)	U (m s^{-1})
1.6	25	66	13.1	0.054
2.4	59	109	8.1	0.054
2	45	66	1.6	0.020
1.68	35	89	11.6	0.015
1.34	38	66	19.8	0.041
1.71	75	57	22.2	0.049
2.28	110	56	20.5	0.059
1.38	95	60	14.5	0.012
2.3	62	77	25.1	0.053
3.29	250	85	11.2	0.010
3.8	90	40	13.2	0.012
1.6	20	22	8.3	0.012
2.2	110	50	6.4	0.012
3.15	91	91	10.3	0.044

PIV, particle image velocimetry; G_{max}, peak mouth gape; T, time to mouth peak gape; v_{max}, maximum velocity of intake flow through the mouth aperture; h_0, initial distance from the plane of the mouth aperture to a plane wall; u, fish speed.

pressure difference δp_B due to the gliding body (Fig. 5). These results depend on swimming speed and the magnitude of suctions flows. For instance, for a fish swimming slowly (~20 mm s^{-1}) at a given distance from the wall, the body-induced wall-detecting signal measured in a neuromast may be an order of magnitude weaker than the suction-induced wall-detecting signal. However, for faster swimming speeds (~100 mm s^{-1}), the two signals may be of the same order of magnitude.

The correlation between swimming speed and the body-induced pressure difference implies an innate trade-off between the strength of the detection signal and the fish's reaction time to avoid an obstacle; speeding up increases the detection signal but reduces the corresponding reaction time. However, the mouth-induced wall-detecting signal depends weakly on the speed of a fish, and therefore it can be useful even when the fish is not moving. This novel finding may provide an alternative explanation to the lack of correlation between swimming speed and turning distance in *A. fasciatus* (Teyke, 1985; Windsor et al., 2008).

In the Earth-fixed frame of references the gliding body of a fish and its mouth suction generate water flow in opposite directions. In the presence of an obstacle and in the frame of reference of the fish, the flow velocity induced by the motion of the body varies slowly in time, whereas that induced by the mouth suction varies rapidly. However, the pressure gradient measured by the canal neuromasts is proportional to the flow acceleration. Thus, even if the two velocities are of the same order of magnitude, their accelerations are not. In this respect, a fish that uses its own gliding body for obstacle detection generates a monotonic and slowly varying disturbance. Multiple mouth suction events generate oscillating signals (Fig. 2 and Fig. 5A). Interestingly, canal neuromasts of *A. fasciatus* are relatively insensitive to slow flow variations but sensitive to oscillating flows (Montgomery et al., 2009; van Netten, 2006). The mouth gape and the related velocity of the suction flows oscillate in time. These oscillating flows can interact with an obstacle to induce an oscillating pressure difference in the canal neuromast. The dominant frequency of these oscillations is of the order of 5–20 Hz (Fig. 5, Table 1), which is close to the lower end of the sensitivity range of the canal neuromasts [10–100 Hz (Montgomery et al., 2009; van Netten, 2006)]. Thus, the stronger signal produced by mouth suction is also more likely to generate a strong neural

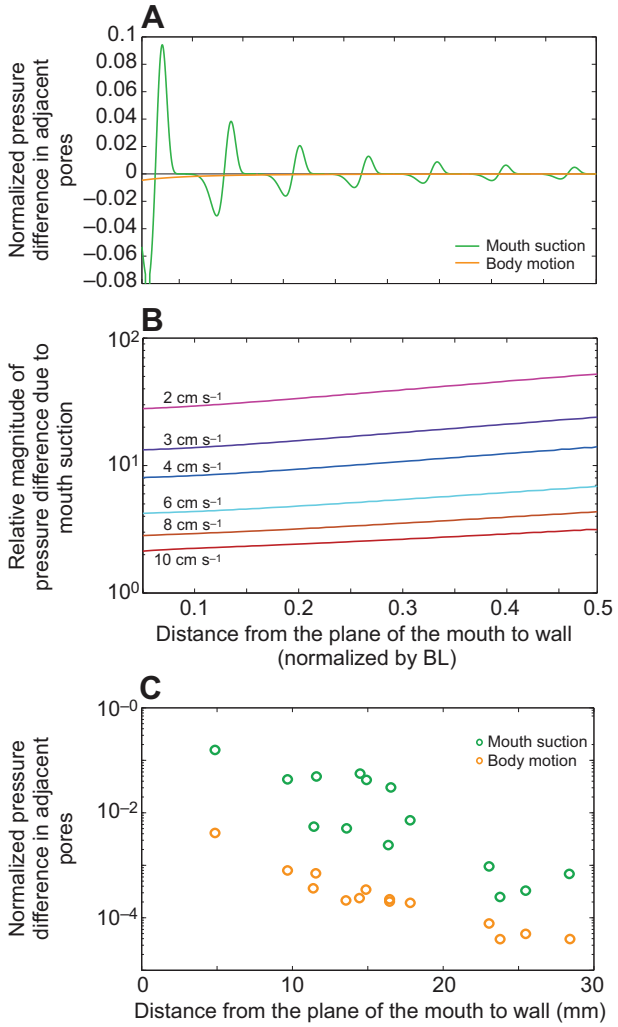

Fig. 5. Pressure difference between adjacent pores as a function of the distance from the mouth aperture to the wall. (A) Simulated pressure differences $\delta p_B(h)$ and $\delta p_S(h)$ are normalized by water density × speed squared (ρU^2). (B) The simulated ratio between pressure difference in two adjacent canal pores due to mouth suction $\delta p_S(h)$ and that due to the gliding body $\delta p_B(h)$ calculated for $h=h_E$ and plotted for different swimming speed U. In A and B the following parameters were adopted: fish length L=5 cm, time to mouth-opening peak gape T=0.078 s, suction fluid velocity v_{max}=0.066 m s^{-1}, maximum mouth gape G_{max}=2.2 mm. The pressure gradient was calculated for a neuromast located at a distance of 0.1L from the plane of the mouth, and the distance between two adjacent pores was δs=0.02L. (C) Simulated values of $|\delta p_B(h_E)|$ and $|\delta p_S(h_E)|$ for 14 mouth-opening events for which PIV data were available (Table 1).

response due to the unsteady flows it produces. It should be stressed that the advantage of the body-induced wall-detecting signal is that it acts continuously, whereas the mouth-induced signal is intermittent and sporadic.

The suction flow creates fluid disturbances in a certain steradian angle, which can be derived from Eqn 6 given in the Appendix. The central axis of the angle is perpendicular to the mouth plane. For a fish moving with its head perpendicular to a wall, the central axis of the steradian angle is also perpendicular to the wall. For small ratios of the mouth diameter to the distance to the obstacle, this angle is small. Therefore, our model of mouth suction flow takes into account only the fluid velocity along the longitudinal axis of the steradian angle. Cases when the fish swim toward the wall at an

angle very different from 90 deg require reformulation of the problem, which is beyond the scope of the present paper.

To detect underwater objects, cetaceans generate high-frequency pressure disturbances that propagate in water as acoustic waves with length much smaller than the distance to a detected object (Friedlander, 1958). Using mouth suction, *A. fasciatus* generates low-frequency pressure oscillation with a wavelength much larger than the distance to the obstacle. In such a case the speed of sound can be considered infinite and the water incompressible (Friedlander, 1958). Thus, the suggested mechanism of obstacle detection using mouth suction by transmitting oscillation signals is clearly not acoustic. However, it does share certain features with echolocation. First, the high-frequency suction flow generated by mouth suction in *A. fasciatus* can be seen as an active emission of obstacle-detection signals, one of the hallmarks of pulse-based navigation mechanisms such as echolocation. Second, a salient feature of echolocation is that animals increase the signal frequency in unfamiliar environments and when approaching a target (Au, 1993; Busnel and Fish, 1980; Simmons et al., 1979; Yovel et al., 2010). Such modulation of mouth-opening frequency was observed in our experiments with Mexican blind cavefish (Fig. 1, Fig. 3B).

The frequency of mouth opening in familiar and unfamiliar environments (0.2–0.7 Hz) is well within the reported range for mouth opening for respiration (Brainerd and Ferry-Graham, 2006; Hughes, 1970; Hughes, 1960). However, our data suggest that the increase in mouth-opening frequency in unfamiliar environments is not due to increased metabolic rates.

First, mouth-opening frequencies near the corner (4.5 Hz; Fig. 3A) were much higher than those observed during slow swimming in other species (Brainerd and Ferry-Graham, 2006; Hughes, 1970; Hughes, 1960). Second, in our experiments, mouth-opening events were 6-fold more likely to occur very close to the corner than at a distance of >7 cm from it, and this modulation is difficult to reconcile with variable metabolic demands over such short distances. Lastly, although we observed a decrease in swimming speed in the unfamiliar environment, *A. fasciatus* was previously observed to swim in an unfamiliar environment at a speed that was 20–30% higher than that observed in a familiar environment (Burt de Perera, 2004; Teyke, 1985). Based on studies in other fish species, such an increase in swimming speed should result in a maximal increase of ~20% in mouth ventilation rate, and sometimes even a decrease in that rate (Altimiras and Larsen, 2000; Clark and Seymour, 2006; Webb, 1971). It is therefore unlikely that the moderate increase in swimming speed previously observed in *A. fasciatus* would result in a 3.5-fold increase in the rate of mouth-opening events, as observed in our experiments.

From a biomechanical perspective, mouth-opening events that generate respiratory and suction-feeding flows are similar (Brainerd and Ferry-Graham, 2006; Westneat, 2006). Both behaviors consist of buccal expansion in order to generate unidirectional water flow through the mouth and out of the operculum. Hydrodynamically, both behaviors generate unsteady flows that can be modeled as passive flow into an orifice. Thus, both are mouth suction behaviors. Evolutionarily, both behaviors are ancestral and conserved across fishes, and have a shared biomechanical and neurological basis (Brainerd and Ferry-Graham, 2006; Westneat, 2006). Consequently, we cannot determine whether using mouth suction to detect obstacles evolved from respiratory or predatory flows. The three behaviors (feeding, respiration and obstacle detection), however, impose specific functional demands on mouth suction flows. In respiratory flows, the efficiency of gas exchange is higher under low flow speeds and weak accelerations (Brainerd and Ferry-Graham, 2006). In contrast, the functional demands for prey capture and obstacle detection by mouth suction are similar, as both depend on fast flows and steep accelerations (Holzman et al., 2012; Holzman et al., 2007; Wainwright et al., 2007). We do not rule out, however, that the mouth suction flows used for obstacle detection are modified respiratory flows, an intermediate behavior between respiratory and prey-capturing flows.

The suggested mechanism of obstacle detection in *A. fasciatus* presents a combination of two ubiquitous mechanisms of ray-finned fishes: the ability to perceive the fluid motion using the lateral line system and the ability to generate unidirectional flows into their mouths. The lateral line system is an ancestral feature of teleosts (Philip et al., 2012), present also in amphibians and Elasmobranchii (Dijkgraaf, 1963). Similarly, the ability to generate mouth suction for prey capture, transport and respiration is ancestral to fishes, and is shared by ray-finned fish, lobe-finned fish, amphibians and elasmobranchs (Lauder, 1982; Lauder, 1985; Westneat, 2006). This constitutes a remarkable example of the evolution of a novel mechanism from a combination of ancient mechanisms originally adopted for other functions. It also implies that this mechanism could be widespread, potentially used by other blind fishes, deep-sea and nocturnal species.

MATERIALS AND METHODS

Filming of fish

Fish were obtained from the pet trade and housed in 400×300×100 mm aquaria for 4–6 weeks before being transferred to the experimental aquaria. Holding aquaria contained a sponge filter, with no additional obstacles. Fish were fed daily with commercial Tetra flakes. The experiments described below complied with IACUC approved guidelines for the use and care of animals in research at Tel Aviv University, Israel.

To characterize mouth opening in *A. fasciatus*, fish (total length L=40–70 mm) were introduced into an experimental aquarium (400×300×100 mm) and filmed using a pair of high-speed (125 frames s^{-1}) synchronized digital video cameras (1280×1024 pixels CMOS, Optronics GmBh, Germany) equipped with 60 mm/f2.8 and 24 mm/f1.8 lenses (Nikkor, Japan). The first camera filmed the aquarium from above while the second had a lateral view of one of the aquarium walls and corners (supplementary material Movie 1). Frame rate was selected such that mouth opening was captured by >4 consecutive frames. The cameras were set to cover an approximately 11×11 cm area of the aquarium, near one of the corners. For the first camera, a grid was placed under the aquarium bottom to calibrate the distances. For the second, a ruler was placed on the aquarium wall near the image boundary. Fish were introduced into the aquarium and immediately filmed when swimming along one of the walls, towards the aquarium corner. From the recorded videos we selected sequences in which the fish was continuously visible through its progress towards the wall (5–20 s long, depending of the fish's swimming speed). For each sequence analyzed, we recorded the time of each mouth-opening event and the distance of the fish from the aquarium wall in front of it. Overall, 123 mouth-opening events were analyzed.

To test whether the frequency of mouth opening in *A. fasciatus* is modulated in unfamiliar environments, we allowed three *A. fasciatus* individuals (total length L=40–70 mm) to acclimate for 48 h in a 400×300×100 mm aquarium. The aquarium contained five cylindrical obstacles of diameter 20–40 mm. Obstacles were made of machined polycarbonate, with a heavy steel base. Oxygen was monitored in the aquarium using YSI ProODO oxygen optode (YSI, Yellow Springs, OH, USA). Following the 48 h acclimation period, fish were filmed from the side at 60 frames s^{-1} for 15 min using a commercial Sony HDR-CX550 camcorder (Sony, Japan). After filming, the obstacles were shifted to arbitrary locations by moving a large magnet under the aquarium, and the fish were filmed again. From the two filming periods (before and after moving the obstacles) we selected short (2–10 s) intervals in which a fish's mouth was continuously observed in the field of view. The number of mouth-opening events in the filming period was quantified, and mouth-opening rate was calculated for each sequence. Overall, we analyzed 30 sequences taken

before obstacle shifting and 31 after. The duration of filming was selected to ensure a large enough sample size for statistical analysis.

We repeated this experiment, using a camera positioned above the aquarium, to quantify the swimming speed of the fish in familiar and unfamiliar environments. Movies were recorded using a GoPro Hero3 camera (San Mateo, CA, USA) recording at 60 frames s^{-1}. We randomly sampled 27 short clips (~1 s) during 5 min prior to obstacle shifting, and 27 short clips (~1 s) during 5 min immediately after obstacle shifting. We determined the swimming speed in each clip by digitizing the fish's head and dividing the cumulative swimming distance by clip duration.

PIV

To characterize the flows produced in front of the mouth due to rapid mouth opening, we used a flow visualization technique termed PIV. The details of this method are described elsewhere (Holzman and Wainwright, 2009; Raffel et al., 1998) and are discussed here only in brief. In general, this technique is used to obtain instantaneous velocity measurements and derived properties in fluids. The fluid is seeded with small, neutrally buoyant particles and is illuminated such that the particles are visible. The motion of the particles is recorded using a high-speed camera, and is analyzed to calculate the speed and direction of the flow in the field of view.

Fish were allowed to acclimate to their aquaria and to the laser sheet described below for a week prior to the PIV experiments. At the onset of each trial, the obstacles were moved to arbitrary locations in the tank. We focused on an area of 5×5 cm near one of the corners of the tank. Fish that swam voluntarily into this area were filmed and their suction flows were analyzed. A Coherent Magnum II 665 nm, 1500 mW solid-state continuous wave laser (fan angle of 10 deg; Coherent Inc., Santa Clara, CA, USA) was used to produce a laser sheet in the experimental aquarium. The laser sheet, ~5 cm wide and 0.1 mm thick, was parallel to the long wall of the aquarium and ~15 mm distant from it. We focused on an area of approximately 50×50 mm, bordering one of the aquarium's corners. The plane of the sheet coincided with the centerline of fish that swam parallel to the wall. To visualize the flow, the water was seeded with 12 µm silver-coated, hollow glass beads with specific gravity of 1.05 (Potter Industries Inc., Carlstadt, NJ, USA). Fish were filmed in lateral view using a high-speed digital video camera (1000 frames s^{-1}, Photron SA-3, Japan) equipped with a 105 mm/f2.8 lens (Nikkor, Japan). Additionally, a camcorder recording at 120 frames s^{-1} (Sony, Japan) captured anterior views of the swimming fish, which were used to verify the orientation and location of the fish within the laser sheet. Sequential images taken during mouth opening, treated as image pairs, were analyzed using a cross-correlation algorithm in MatPIV (http://folk.uio.no/jks/matpiv/index2.html), an open software toolbox for PIV analysis in MATLAB (MathWorks Inc., MA, USA). Image pairs were analyzed using a windows shifting technique, starting with 64×64 pixel interrogation areas and ending with 16×16 pixel areas (with 50% overlap) after six passes. The cross-correlation algorithm returned a two-dimensional grid of vertical and horizontal velocities and signal-to-noise ratio (SNR) for each image pair analyzed.

We extracted data on the magnitude of flow speed at the center of the mouth at each time point. Velocity values with an SNR value lower than 2 were omitted (<10% of the cases). We define peak flow speed as the maximum flow speed observed during a mouth-opening event. We analyzed only sequences in which the laser sheet intersected with the mid-sagittal plane of the fish, as verified with the anterior view camera. In addition to the calculation of flow speed, we determined for each frame the longitudinal and transverse coordinates of the anterior-most points on the fish's upper and lower jaws, using the MATLAB free package DLTdv5 (Hedrick, 2008). We used these landmarks to calculate gape distance and gape angle, the angle between the upper and lower jaw. We also calculated the time to mouth opening, defined as the time it takes the fish to open its mouth from 20% to 95% of the maximal gape observed during the mouth-opening event (Holzman et al., 2008). Overall, we analyzed 14 mouth-opening events for the three fish.

Statistical analysis

We used Bartlett's test for homogeneity of variance implemented in the software R statistics (R Development Core Team, 2009) to determine whether variation in mouth-opening frequency differed significantly between individuals. A fast Fourier transform (FFT) algorithm implemented in MATLAB was used on sequences of repeated mouth opening to estimate the dominant frequency of these events. A chi-square test was used to test whether the frequency of mouth-opening events was higher at different distances from the corner by comparing the observed frequencies to a uniform distribution (same number of events in each distance category). Unless otherwise stated, statistical tests were carried out using the software R statistics (R Development Core Team, 2009). Throughout the text, means are shown ±s.d.

A mathematical model of obstacle detection using mouth suction

The primary aim of our modeling was to clarify mathematically which of the physical processes, the steadily gliding body of a fish or its unsteady mouth suction, generates stronger wall-detection signals that can be sensed by the lateral line. For this purpose we use the premises of inviscid incompressible fluid, the closed-form expressions for the hydrodynamic field generated by a moving ellipsoid (Milne-Thomson, 1968) and the closed-form expressions for the hydrodynamic field generated by a disk of sinks (Lamb, 1932). Using the method of hydrodynamic images, we calculated the pressure that is induced by the wall in two adjacent canal pores for a fish moving perpendicular to the wall. We then compared the magnitude of the pressure differences in two adjacent canal pores generated by the two mechanisms.

The parameters used for our mathematical modeling are the following: fish length L, the speed of fish U, peak mouth opening G_{max}, time to peak gape T, the peak velocity of intake flows at the center of the mouth aperture v_{max} and the minimal distance h_{min} at which a Mexican blind fish starts the wall-avoiding maneuver. The typical characteristic scales were adopted here for numerical calculations: L=50 mm, U=20–1000 mm s^{-1}, h_{min}=5 mm (e.g. Windsor et al., 2008). For numerical estimates of T, G_{max} and v_{max} we used the values measured in our filming and PIV measurements (see Results, 'Experimental results'): G_{max}=2.2 mm, v_{max}=66 mm s^{-1} and T=0.078 s (see Results).

For the range of swimming speeds adopted here, the Reynolds numbers $Re=UL/\nu$=2000–10,000 is sufficiently low to assume that a fish's body boundary layer is laminar and thin (Schlichting, 1979; Vogel, 1994). In such a case, according to the basic assumptions of the boundary layer theory, the flow outside the boundary layer can be considered as inviscid and irrotational (potential) (Schlichting, 1979). The distance in front of the mouth aperture, where the viscosity influences the velocity field due to mouth suction $\sqrt{(\nu T)}\approx 0.3$ mm (Tuck, 1970), is much smaller than h_{min}=5 mm. Therefore, we also considered the flow generated by the mouth aperture as inviscid and potential.

Given that pores of canal neuromasts are spaced at relatively small intervals δs with respect to the fish's length (Schemmel, 1967), the pressure difference in a neuromast can be approximated as:

$$\Delta p = \delta \mathbf{s} \times \nabla p \ , \quad (1)$$

where $\delta \mathbf{s}$ is the vector connecting two adjacent pores and ∇p is the pressure gradient. In the Earth-bound frame of reference the equation of motion of inviscid incompressible fluid can be described by the Euler and continuity equations (Milne-Thomson, 1968):

$$\frac{\partial \mathbf{V}}{\partial t} + (\mathbf{V} \times \nabla)\mathbf{V} = -\frac{1}{\rho}\nabla p \ , \quad (2)$$

$$\nabla \times \mathbf{V} = 0 \ , \quad (3)$$

where ρ is the fluid density and t is time.

If a body moves in an unbounded fluid with constant velocity U then, in the frame of reference attached to the body, the fluid motion is steady, and the local fluid acceleration $\partial \mathbf{V}/\partial t$ on the left-hand side of Eqn 2 vanishes. If a body approaches a wall, the geometry of the fluid domain varies in time, the fluid velocity becomes time dependent, and the fluid acceleration in Eqn 2 becomes non-zero. It is important to note that the fluid acceleration may also become non-zero as a result of unsteady mouth suction.

Consider a fish moving with constant velocity in the direction normal to an infinite plane wall. Assume that the velocity field created by a fish in unbounded fluid is known. To satisfy the conditions of impermeability on the wall exactly and on the fish body approximately, we used the method of mirror

The Journal of Experimental Biology (2014) doi:10.1242/jeb.098384

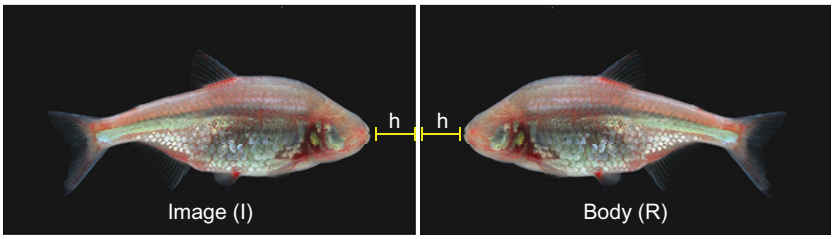

Fig. 6. The method of hydrodynamic images. In the frame of reference attached to a wall, fish *R* moves with speed *U* towards the wall bounding the right half-space. Fish *I*, a mirror image of *R* with respect to the wall, moves with the same speed *U* but in the opposite direction. Because of symmetry, the fluid velocity normal to the plane that separates the two fish is zero. Fish *I* induces in the neuromast fish *R* the same stimuli that are induced by the wall.

images (Milne-Thomson, 1968), where the hydrodynamic combination 'fish–wall' is replaced by two identical fish '*R*+*I*' swimming in unbounded fluid along the same line with the same velocity *U* but in opposite directions, where *I* is a mirror image of *R* with respect to the wall (Fig. 6). We further assume that fish *R* is fixed in space and that the water moves with constant velocity *U* directed from the fish's head to its tail; whereas the fish image *I* moves with velocity 2*U* with respect to *R* and with velocity *U* with respect to water. The moving fish *I* generates water disturbances by its gliding body or by its mouth suction. These disturbances create pressure gradients ∇p in the neuromasts of *R*, which are identical to ∇p created in the same neuromasts by the wall in the combination '*R*+wall'. Once ∇p is defined, the pressure difference in two adjacent pores is also defined by Eqn 2.

We further used two orthogonal coordinate systems, O_1xyz fixed in non-moving fish *R* and $O\xi\eta\zeta$ fixed in moving fish *I* ($O_1x \| O\xi$, $O_1y \| O\eta$ and $O_1z \| O\zeta$). The axes O_1x and $O\xi$ are collinear with *U*. The relationship between the two coordinate systems is $\xi = x - 2Ut + h_0$, where h_0 is the distance between *O* and O_1 at the initial moment of time $t=0$. Assume that the fluid velocity of fluid disturbances generated by the fish image *I* in an unbounded domain is known in the fixed coordinate system $O\xi\eta\zeta$. The total vector of the fluid in the fixed-in-space coordinate system O_1xyz can be represented as:

$$\mathbf{V}(x, y, z) = \mathbf{U} + \mathbf{V}_B(x - 2Ut, y, z, t) + \mathbf{V}_S(x - 2Ut, y, z, t) \,, \quad (4)$$

where $\mathbf{V}_B$ is the fluid velocity of fluid disturbances pertaining to the gliding body and $\mathbf{V}_S$ to the mouth suction. Assume that the fish is a slender and streamlined body which generates weak fluid disturbances $|\mathbf{V}_{B,S}| \ll U$. Then, substituting Eqn 4 into Eqn 2, and neglecting higher order terms, we can decompose the pressure gradients into the pressure gradients pertaining to a fish's gliding body, and to that pertaining to the mouth suction.

To calculate the fluid disturbances generated by a fish's gliding body, we replaced it with a three-dimensional ellipsoid $\xi^2/a^2+\eta^2/b^2+\zeta^2/c^2=1$ moving in unbounded fluid with velocity *U* directed along the axis $O\xi$ (supplementary material Fig. S1).

The algorithm for calculating the corresponding fluid velocities that result from the motion of an ellipsoid (Milne-Thomson, 1968) is provided in the Appendix.

We consider the flow created by mouth suction as that created by a disk of sinks of uniform density over the plane area contained by a circle $\eta^2+\zeta^2=r^2(t)$ (Lamb, 1932), where the radius of the disk *r* varies in time as:

$$r(t) = f(t)\frac{G_{\max}}{2} \,, \quad (5)$$

$$G_{\max} = G(t)\big|_{t=T} \,, \quad (6)$$

$$f(t) = \begin{cases} (\tau e^{1-\tau})^{\alpha} & \text{for } \tau > 0 \\ 0 & \text{for } \tau \le 0 \end{cases} \,, \quad (7)$$

$\tau=(t-t_0)/T$, t_0 is the initial time of suction and $\alpha \approx 5$ is an experimental fitting parameter. The total flow rate $\dot{q}$ through the circle can be estimated using PIV measurements of the suction velocity $v_{\max}f(t)$ in the center of the mouth aperture:

$$\dot{q} = \pi\, v_{\max} f(t) r^2 \,. \quad (8)$$

The fluid velocity on the central axis of the disk $O\xi$ can be written as:

$$u = -v_{\max} f(t)\left[1 - \frac{\xi^+}{\sqrt{1+\xi^{+2}}}\right], \quad (9)$$

where ξ^+ is the distance from the plane of mouth to the point of a fluid normalized with the radius $r(t)$ (see Appendix). Eqn 9 captures the main spatial and temporal characteristics of the velocity field created by mouth suction (Day et al., 2005; Day et al., 2007; Holzman et al., 2008; Muller et al., 1982) (supplementary material Fig. S2). Once the fluid components of the disk-induced flow are known, the disk-induced velocity vector and its derivative with respect to time are also defined.

APPENDIX

To calculate the fluid velocities, we used the theory of potential flow (Milne-Thomson, 1968) where the fluid velocity is calculated as a gradient of the fluid velocity potential. Once the fluid velocity potential is known, the fluid velocity field is also known. The fluid velocity potential of an ellipsoid moving along its longitudinal axis is given as (Milne-Thomson, 1968):

$$\varphi_B = k\xi A(\lambda) \,, \quad (A1)$$

where:

$$A(\lambda) = abc\int_{\lambda}^{\infty} \frac{dq}{(a^2+q)\sqrt{(a^2+q)(b^2+q)(c^2+q)}} \,, \quad (A2)$$

$\lambda=\lambda(\xi, y, \zeta)$ is the positive real root of an algebraic equation:

$$\frac{\xi^2}{a^2+\lambda} + \frac{\eta^2}{b^2+\lambda} + \frac{\zeta^2}{c^2+\lambda} = 1 \,, \quad (A3)$$

$k=-U/(2-A_0)$ and A_0 is the value of *A* for $\lambda=0$. The fluid velocity components induced by the motion of the ellipsoid can be bound from Eqns A1, A2 as:

$$\frac{\partial\varphi_B}{\partial\xi} = k\left(A + \xi\frac{\partial A}{\partial\lambda}\frac{\partial\lambda}{\partial\xi}\right), \frac{\partial\varphi_B}{\partial\eta} = k\xi\frac{\partial A}{\partial\lambda}\frac{\partial\lambda}{\partial\eta}, \frac{\partial\varphi_B}{\partial\zeta} = k\xi\frac{\partial A}{\partial\lambda}\frac{\partial\lambda}{\partial\zeta} \,. \quad (A4)$$

The derivatives $\partial\lambda/\partial\xi$, $\partial\lambda/\partial\eta$ and $\partial\lambda/\partial\zeta$ can be obtained by differentiating Eqn A3 with respect to ξ, η, ζ. For instance, differentiation with respect to ξ gives the following linear equation with respect to $\partial\lambda/\partial\xi$:

$$\frac{2\xi}{a^2+\lambda} - \left(\frac{\xi^2}{a^2+\lambda} + \frac{\eta^2}{b^2+\lambda} + \frac{\zeta^2}{c^2+\lambda}\right)\frac{\partial\lambda}{\partial\xi} = 0 \,, \quad (A5)$$

the solution of which is straightforward. Thus, calculating the fluid velocity components induced by image *I* on the surface of *R* is reduced to a numeric solution of an algebraic Eqn A3 and numeric calculation of Eqn A2.

We consider the flow created by mouth suction as that created by a disk of sinks of uniform density over the plane area contained by a circle $\eta^2+\zeta^2=r^2(t)$, where the radius *r* varies in time. The fluid velocity potential φ_S induced by the disk of sinks can be written as (Lamb, 1932):

$$\varphi_S(\xi_1, \eta, \zeta, t) = -\frac{q}{\pi r}\int_0^{\infty} e^{-k\xi_1} J_0(k\bar{\omega}) J_1(kr)\frac{dk}{k} \quad (\xi_1 \ge 0) \,, \quad (A6)$$

where ξ_1 is the distance from the disk to the field point, and $\bar{\omega}=\sqrt{(\eta^2+\zeta^2)}$ and $J_{0,1}$ are the Bessel functions of the first kind of a real argument. Differentiation of Eqn A6 with respect to ξ_1, η and ζ yields the fluid velocity components induced by the disk of sources. For instance, given that $J_0(0)=1$, the fluid velocity on the central axis of the disk $O\xi_1$ ($\bar{\omega}=0$) can be written as:

$$u=\left.\frac{\partial\varphi}{\partial\xi_1}\right|_{\bar{r}=0}=\frac{q}{\pi r}\int_0^{\infty}e^{-k\xi_1}J_1(kr)\,\mathrm{d}k=-v_{\max}f(t)\left[1-\frac{\xi^+}{\sqrt{1+\xi^{+2}}}\right], \quad \text{(A7)}$$

where $\xi^+=\xi_1/r$ (supplementary material Fig. S2).

Acknowledgements
We thank Anatoli Zapolski for his help with filming experiments. We are indebted to Amatzia Genin, Matt McHenry, Victor Mishkevich, Peter Wainwright and Yossi Yovel for discussions and comments on the manuscript.

Competing interests
The authors declare no competing financial interests.

Author contributions
R.H. and G.Z. conceived and designed the research; R.H., G.Z. and S.P.F. conducted the experiments; R.H., S.P.F. and G.Z. analyzed the results; G.Z. carried out the mathematical modelling; R.H. and G.Z. wrote the paper.

Funding
The study was funded by Israeli Science Foundation (ISF) 158/11 to R.H.

Supplementary material
Supplementary material available online at
http://jeb.biologists.org/lookup/suppl/doi:10.1242/jeb.098384/-/DC1

References

Abdel-Latif, H., Hassan, E. S. and von Campenhausen, C. (1990). Sensory performance of blind Mexican cave fish after destruction of the canal neuromasts. *Naturwissenschaften* **77**, 237-239.
Altimiras, J. and Larsen, E. (2000). Non-invasive recording of heart rate and ventilation rate in rainbow trout during rest and swimming. Fish go wireless! *J. Fish Biol.* **57**, 197-209.
Au, W. W. L. (1993). *The Sonar of Dolphins*. New York, NY: Springer.
Bleckmann, H. (2007). The lateral line system of fish. In *Fish Physiology*, Vol. 25 (ed. J. H. Toshiaki and S. Z. Barbara), pp. 411-453. Waltham, MA: Academic Press.
Brainerd, E. L. and Ferry-Graham, L. (2006). Mechanics of Respiratory Pumps. In *Fish Physiology: Fish Biomechanics: Fish Biomechanics*, Vol. 23 (ed. R. E. Shadwick and G. V. Lauder). London: Elsevier.
Burt de Perera, T. (2004). Spatial parameters encoded in the spatial map of the blind Mexican cave fish, *Astyanax fasciatus*. *Anim. Behav.* **68**, 291-295.
Busnel, R. G. and Fish, J. (1980). *Animal Sonar Systems*. New York, NY: Plenum.
Campenhausen, C., Riess, I. and Weissert, R. (1981). Detection of stationary objects by the blind cave fish *Anoptichthys jordani* (Characidae). *J. Comp. Physiol. A* **143**, 369-374.
Clark, T. D. and Seymour, R. S. (2006). Cardiorespiratory physiology and swimming energetics of a high-energy-demand teleost, the yellowtail kingfish (*Seriola lalandi*). *J. Exp. Biol.* **209**, 3940-3951.
Day, S. W., Higham, T. E., Cheer, A. Y. and Wainwright, P. C. (2005). Spatial and temporal patterns of water flow generated by suction-feeding bluegill sunfish *Lepomis macrochirus* resolved by particle image velocimetry. *J. Exp. Biol.* **208**, 2661-2671.
Day, S. W., Higham, T. E. and Wainwright, P. C. (2007). Time resolved measurements of the flow generated by suction feeding fish. *Exp. Fluids* **43**, 713-724.
Denton, E. J. and Gray, J. A. B. (1982). The rigidity of fish and patterns of lateral line stimulation. *Nature* **297**, 679-681.
Denton, E. J. and Gray, J. (1983). Mechanical factors in the excitation of clupeid lateral lines. *Proc. R. Soc. B* **218**, 1-26.
Denton, E. and Gray, J. (1988). Mechanical factors in the excitation of the lateral lines of fishes. In *Sensory Biology of Aquatic Animals*, Vol. 1 (ed. J. Atema, R. R. Fay, A. N. Popper and W. N. Tavolga), pp. 595-617. New York, NY: Springer-Verlag.
Denton, E. and Gray, J. (1989). Some observations on the forces acting on neuromasts in fish lateral line canals. In *The Mechanosensory Lateral Line. Neurobiology and Evolution* (ed. S. Coombs, P. Gorner and H. Munz), pp. 239-246. New York, NY: Springer-Verlag.
Dijkgraaf, S. (1933). Untersuchungen über die Funktion der Seitenorgane an Fischen. *J. Comp. Physiol. A* **20**, 162-214.
Dijkgraaf, S. (1947). Über die reizung des ferntastsinns bei fischen und amphibien. *Cell. Mol. Life Sci.* **3**, 206-208.
Dijkgraaf, S. (1963). The functioning and significance of the lateral-line organs. *Biol. Rev. Camb. Philos. Soc.* **38**, 51-105.
Friedlander, F. G. (1958). *Sound Pulses*. Cambridge: Cambridge University Press.
Gibb, A. C. and Ferry-Graham, L. (2005). Cranial movements during suction feeding in teleost fishes: Are they modified to enhance suction production? *Zoology* **108**, 141-153.
Hedrick, T. L. (2008). Software techniques for two- and three-dimensional kinematic measurements of biological and biomimetic systems. *Bioinspir. Biomim.* **3**, 034001.
Higham, T. E., Day, S. W. and Wainwright, P. C. (2006). The pressures of suction feeding: the relation between buccal pressure and induced fluid speed in centrarchid fishes. *J. Exp. Biol.* **209**, 3281-3287.
Holzman, R. and Wainwright, P. C. (2009). How to surprise a copepod: Strike kinematics reduce hydrodynamic disturbance and increase stealth of suction-feeding fish. *Limnol. Oceanogr.* **54**, 2201-2212.
Holzman, R., Day, S. W. and Wainwright, P. C. (2007). Timing is everything: coordination of strike kinematics affects the force exerted by suction feeding fish on attached prey. *J. Exp. Biol.* **210**, 3328-3336.
Holzman, R., Collar, D. C., Day, S. W., Bishop, K. L. and Wainwright, P. C. (2008). Scaling of suction-induced flows in bluegill: morphological and kinematic predictors for the ontogeny of feeding performance. *J. Exp. Biol.* **211**, 2658-2668.
Holzman, R., Collar, D. C., Mehta, R. S. and Wainwright, P. C. (2012). An integrative modeling approach to elucidate suction-feeding performance. *J. Exp. Biol.* **215**, 1-13.
Hughes, G. M. (1960). A comparative study of gill ventilation in marine teleosts. *J. Exp. Biol.* **37**, 28-45.
Hughes, G. M. (1970). A comparative approach to fish respiration. *Experientia* **26**, 113-122.
Kroese, A. B. and Schellart, N. A. (1992). Velocity- and acceleration-sensitive units in the trunk lateral line of the trout. *J. Neurophysiol.* **68**, 2212-2221.
Lamb, H. (1932). *Hydrodynamics*. New York, NY: Dover.
Lauder, G. V. (1980). Hydrodynamics of prey capture in teleost fishes. In *Biofluid Mechanics*, Vol. II (ed. D. Schenck), pp. 161-181. New York, NY: Plenum Press.
Lauder, G. V. (1982). Patterns of evolution in the feeding mechanism of actinopterygian fishes. *Am. Zool.* **22**, 275-285.
Lauder, G. V. (1985). Aquatic feeding in lower vertebrates. In *Functional Vertebrate Morphology* (ed. M. Hildebrand, D. M. Bramble, K. F. Liem and D. B. Wake), pp. 210-229. Cambridge, MA: Harvard University Press.
Milne-Thomson, L. M. (1968). Theoretical hydrodynamics. London: Macmillan.
Montgomery, J., Coombs, S. and Halstead, M. (1995). Biology of the mechanosensory lateral line in fishes. *Rev. Fish Biol. Fish.* **5**, 399-416.
Montgomery, J. C., Coombs, S. and Baker, C. F. (2001). The mechanosensory lateral line system of the hypogean form of astyanax fasciatus. *Environ. Biol. Fishes* **62**, 87-96.
Montgomery, J. C., Windsor, S. and Bassett, D. (2009). Behavior and physiology of mechanoreception: separating signal and noise. *Integrative Zoology* **4**, 3-12.
Muller, M., Osse, J. W. M. and Verhagen, J. H. G. (1982). A quantitative hydrodynamical model of suction feeding in fish. *J. Theor. Biol.* **95**, 49-79.
Nauwelaerts, S., Wilga, C., Sanford, C. and Lauder, G. (2007). Hydrodynamics of prey capture in sharks: effects of substrate. *J. R. Soc. Interface* **4**, 341-345.
Philip, S., Machado, J. P., Maldonado, E., Vasconcelos, V., O'Brien, S. J., Johnson, W. E. and Antunes, A. (2012). Fish lateral line innovation: insights into the evolutionary genomic dynamics of a unique mechanosensory organ. *Mol. Biol. Evol.* **29**, 3887-3898.
R Development Core Team (2009). *R: A Language and Environment for Statistical Computing*. Vienna, Austria: R Foundation for Statistical Computing.
Raffel, M., Willert, C. E. and Kompenhans, J. (1998). *Particle Image Velocimetry: A Practical Guide*. Berlin: Springer.
Schemmel, C. (1967). Vergleichende untersuchungen an den hautsinnesorganen ober- und unterirdisch lebender astyanax-formen. *Zoomorphology* **61**, 255-316.
Schlichting, H. (1979). *Boundary Layer Theory*. New York, NY: McGraw-Hill.
Simmons, J. A., Fenton, M. B. and O'Farrell, M. J. (1979). Echolocation and pursuit of prey by bats. *Science* **203**, 16-21.
Teyke, T. (1985). Collision with and avoidance of obstacles by blind cave fish *Anoptichthys jordani* (Characidae). *J. Comp. Physiol. A* **157**, 837-843.
Tuck, E. O. (1970). Unsteady flow of a viscous fluid from a source in a wall. *J. Fluid Mech.* **41**, 641-652.
van Netten, S. M. (2006). Hydrodynamic detection by cupulae in a lateral line canal: functional relations between physics and physiology. *Biol. Cybern.* **94**, 67-85.
Van Wassenbergh, S. and Aerts, P. (2009). Aquatic suction feeding dynamics: insights from computational modelling. *J. R. Soc. Interface* **6**, 149-158.
Vogel, S. (1994). *Life in Moving Fluids*. Princeton, NJ: Princeton University Press.
Wainwright, P., Carroll, A. M., Collar, D. C., Day, S. W., Higham, T. E. and Holzman, R. A. (2007). Suction feeding mechanics, performance, and diversity in fishes. *Integr. Comp. Biol.* **47**, 96-106.
Webb, P. W. (1971). The swimming energetics of trout. I. Thrust and power output at cruising speeds. *J. Exp. Biol.* **55**, 489-520.
Weihs, D. (1980). Hydrodynamics of suction feeding of fish in motion. *J. Fish Biol.* **16**, 425-433.
Westneat, M. W. (2006). Skull biomechanics and suction feeding in fishes. In *Fish Biomechanics* (ed. G. V. Lauder and R. E. Shadwick), pp. 29-75. San Diego, CA: Elsevier Academic Press.
Windsor, S. P., Tan, D. and Montgomery, J. C. (2008). Swimming kinematics and hydrodynamic imaging in the blind Mexican cave fish (Astyanax fasciatus). *J. Exp. Biol.* **211**, 2950-2959.
Windsor, S. P., Norris, S. E., Cameron, S. M., Mallinson, G. D. and Montgomery, J. C. (2010). The flow fields involved in hydrodynamic imaging by blind Mexican cave fish (*Astyanax fasciatus*). Part I: open water and heading towards a wall. *J. Exp. Biol.* **213**, 3819-3831. http://dx.doi.org/10.1242/jeb.040741
Yovel, Y., Falk, B., Moss, C. F. and Ulanovsky, N. (2010). Optimal localization by pointing off axis. *Science* **327**, 701-704.